arXiv:1212.5696v1 [cond-mat.mtrl-sci] 22 Dec 2012

Measuring excitation-energy transfer with a real-time time-dependent density functional theory approach

D. Hofmann[1], H. Appel[2,3,4], M. Di Ventra[3], and S. Kümmel[1]
[1] *Theoretical Physics IV, University of Bayreuth, D-95440 Bayreuth, Germany*
[2] *Fritz-Haber-Institut der Max-Planck-Gesellschaft, Faradayweg 4-6, D-14195 Berlin, Germany*
[3] *University of California San Diego, La Jolla, CA 92093, USA and*
[4] *European Theoretical Spectroscopy Facility*

(Dated: December 27, 2012)

We investigate the time an electronic excitation travels in a supermolecular setup using a measurement process in an open quantum-system framework. The approach is based on the stochastic Schrödinger equation and uses a Hamiltonian from time-dependent density functional theory (TDDFT). It treats electronic-structure properties and intermolecular coupling on the level of TDDFT, while it opens a route to the description of dissipation and relaxation via a bath operator that couples to the dipole moment of the density. Within our study, we find that in supermolecular setups small deviations of the electronic structure from the perfectly resonant case have only minor influence on the pathways of excitation-energy transfer, thus lead to similar transfer times. Yet, sizable defects cause notable slowdown of the energy spread.

PACS numbers: 31.70.Hq, 31.15.ee, 82.20.Wt

I. INTRODUCTION

Electronic excitation-energy transfer (EET) after light absorption is one of the key processes in the natural light harvesting (LH) event and a prerequisite for charge generation in the LH reaction center [1, 2]. Hence, it enables efficient energy recovery in biological systems. The efficiency of the light harvesting process is determined by the rates of charge transfer and EET of many single transfer steps contributing to the entire mechanism. In multichromophoric supermolecules as for instance LH systems, such rates are affected by a number of different properties and phenomena: the electronic structure of the single chromophores, the electronic coupling between different system components, the geometry and arrangement of all constituents, the energetic and position (dis)order, and the interplay with the environment.

Recent investigations of the natural LH event have emphasized the importance of quantum-mechanical effects to the LH mechanism [3–8] and are exploring the existence of long-lived quantum coherences during the EET process even at ambient temperature conditions [9–16]. The character of these coherences, i.e., the question whether they are of electronic or vibronic nature, is a controversy in the field [17–21]. The quantum-coherent energy transfer is understood to direct and hence support energy flow within the ring system of LH antenna complexes [2, 8, 9, 12]. Also in artificial π-conjugated polymers, similar quantum-coherence effects have been found [22–25]. Thus, quantum-mechanical interference of energy-transfer pathways plays a prominent role to obtain results beyond the classical laws of probability [8] and may improve the efficiency of intrachain energy migration [22]. Hope is high that a deep understanding of the fundamental design principles of natural LH complexes provides tailored concepts for the design of artificial organic devices [15, 26, 27].

The role of coherent energy transfer and the environment of the system has been studied theoretically based on the density-matrix formalism where usually the models of Haken and Stobl, the model of Redfield, polaron modifications, or related theories are employed [5, 28–35]. Such approaches rely on input from electronic-structure theory or from the experiment. In the present manuscript, we provide an alternative to the previous approaches: We address the energy-transfer problem directly on the level of electronic-structure theory using time-dependent density functional theory (TDDFT) [36–41] in real time. The strengths of TDDFT in the context of EET are versatile. First, in principle it allows for an exact treatment of the electronic structure including electronic excitations and couplings between fragments of supermolecular setups. Second, TDDFT is able to deal with multichromophoric systems of practical relevance on a first-principles level at bearable computational cost. Yet, the validity of TDDFT results strongly depends on the quality of the underlying approximations for exchange-correlation (xc) effects. Therefore, work is going on to improve the reliability of currently available xc functionals [41–48]. Based on a given xc functional, TDDFT allows for a transparent analysis of the influence of electronic-structure properties on EET in sizable molecular systems.

The standard TDDFT approach rests upon closed quantum-system time-dependent Kohn-Sham (TDKS) equations that evolve coherently in time. It does not comply with experimental situations that involve energy dissipation and/or decoherence. Therefore, to investigate the real-time dynamics of a system in contact with a dissipative bath, one needs to go beyond standard TDDFT and use open quantum-system schemes [49–64]. The approach that we employ in the present work is embedded in the framework of TDDFT and uses stochastic TDKS equations [50–55].

The aim of our work is to investigate the coherent EET process in a ring configuration of model molecules in the spirit of the circular LH complexes. In this setup, we exploit the strengths of TDDFT and examine the influence of intermolecular coupling as well as energetic disorder and mismatch. To this end, we introduce an effective bath operator that plays the role of a measurement process to determine the time, a dipolar excitation is travelling in the molecular assembly before it dissipates. It couples to the dipole moment of the supermolecule or appropriate subsystems of the latter. We use this measurement process to deexcite the system, thus remove the entire excitation energy. Note, that in real systems excitation energy transfer may also occur to the environment, e.g., to neighboring complexes and/or may dissipate to nuclear degrees of freedom.

The paper is organized as follows. In Sec. II we outline the stochastic TDKS approach and introduce a bath operator that couples to the dipole moment. More insight into our single-particle scheme is provided in Appendix A. The model system investigated in this manuscript is introduced in Sec. III where we also examine the performance of the bath operator. Moreover, we explain the idea of using the bath operator in the sense of a measurement process to determine the effective time an excitation can travel in a supermolecular system before deexcitation occurs. Details about the electronic structure of the subsystems and the intermolecular coupling in the supermolecule are compiled in Appendix B. We introduce our method to obtain these properties in Appendix C. In Sec. IV, we report our results on the influence of varying electronic-structure properties and different intermolecular coupling mechanisms on EET times in the model system. Finally, we summarize and conclude our findings in Sec. V.

II. DISSIPATION IN REAL-TIME TIME-DEPENDENT DENSITY FUNCTIONAL THEORY

A. Stochastic Schrödinger equation

One of the most basic ideas of open quantum-system treatments is to split the entire Hamiltonian into system, bath, and system-bath interaction contributions

$$\hat{H} = \hat{H}_{\mathrm{S}} \otimes \hat{I}_{\mathrm{B}} + \hat{I}_{\mathrm{S}} \otimes \hat{H}_{\mathrm{B}} + \lambda \hat{H}_{\mathrm{SB}}. \tag{1}$$

$\hat{I}_{\mathrm{S}}$ and $\hat{I}_{\mathrm{B}}$ denote identities in the system (S) and bath (B) Hilbert spaces. The system includes all dynamics and observables of the core system, e.g., of one molecular complex. The bath and system-bath coupling describe the environment as for example surrounding molecules and its interactions with the core system part. Here, the system degrees of freedom are coupled to a bosonic environment. The system of interest is described by the electronic many-particle Hamiltonian

$$\begin{aligned} \hat{H}_{\mathrm{S}} =& \sum_i \left[\frac{[\hat{\mathbf{p}}_i + \hat{\mathbf{A}}_{\mathrm{ext}}(\hat{\mathbf{r}}_i, t)]^2}{2m} + \hat{v}_{\mathrm{ext}}(\hat{\mathbf{r}}_i, t) \right] \\ &+ \sum_{i<j} \hat{W}(\hat{\mathbf{r}}_i - \hat{\mathbf{r}}_j), \end{aligned} \tag{2}$$

where $\mathbf{A}_{\mathrm{ext}}$ is an external vector potential, v_{ext} a scalar external potential, and $\hat{W}$ describes the particle-particle interaction. The environment, given by $\hat{H}_{\mathrm{B}}$, induces a fluctuating force that drives the system due to the interaction

$$\hat{H}_{\mathrm{SB}} = \sum_{\alpha} \hat{S}_{\alpha} \otimes \hat{B}_{\alpha} \tag{3}$$

between the system and the bath. The latter is expressed by many-particle operators $\hat{S}_{\alpha}$ and $\hat{B}_{\alpha}$ in the most general case, where $\hat{S}_{\alpha}$ operates on the system degrees, $\hat{B}_{\alpha}$ on the bath degrees of freedom, and α denotes different possible system-bath coupling mechanisms. The bath may have a complex structure and not all of its microscopic details are relevant for the system dynamics. The driving force that is induced by the bath may, therefore, be subsumed by stochastic fluctuation and dissipation contributions that can usually be characterized by mean values and correlation functions [66]. The parameter λ determines the strength of the system-bath interaction and can be used as an expansion parameter in the weak coupling regime.

The stochastic Schrödinger equation (SSE) and quantum master equations are approaches to describe the dynamics of such a core quantum system in contact with an external bath [54, 55, 65–69]. While quantum master equation approaches are based on density matrices, the SSE uses a statistical ensemble of state vectors to unravel the open quantum-system dynamics directly on the level of wave functions. A noteworthy difference between between the SSE and Redfield and similar master-equation-type approaches is related to the statistical operator. In the latter methods, positivity of the statistical operator may not be guaranteed in cases of stochastic Hamiltonians, time-dependent (TD) Hamiltonians, or TD bath operators [51, 59, 70]. However, the positivity issue does not arise in the SSE. It yields normalized wave functions with a positive weight for arbitrary TD operators. This aspect is particularly important if one intends to use Hamiltonians from density functional theory (DFT) [51, 59] as we do in the following sections. Therefore, the SSE is a solid starting point for a (TD)DFT theory of open quantum systems.

The open quantum-system approach that is applied throughout this work is based on the SSE in the so-called Born-Markov limit [54, 55, 65–69]

$$\begin{aligned} \text{ß}\partial_t \Psi_{\mathrm{S}}(t) =& \hat{H}_{\mathrm{S}}(t)\Psi_{\mathrm{S}}(t) - \frac{\text{ß}}{2} \sum_{\alpha} \hat{S}_{\alpha}^{\dagger} \hat{S}_{\alpha} \Psi_{\mathrm{S}}(t) \\ &+ \sum_{\alpha} l_{\alpha}(t) \hat{S}_{\alpha} \Psi_{\mathrm{S}}(t), \end{aligned} \tag{4}$$

where $l_\alpha(t)$ are stochastic processes with vanishing ensemble average and δ-time-correlation

$$\overline{l_\alpha(t)} = 0,\ \overline{l_\alpha(t)l_\beta(t')} = 0,\ \overline{l_\alpha^*(t)l_\beta(t')} = \delta_{\alpha\beta}\delta(t-t'). \quad (5)$$

The bar denotes the statistical average over an ensemble of stochastic processes. For the sake of convenience, the coupling strength parameter λ has been absorbed in the bath operator $\hat{S}_\alpha$. The first term of the SSE (4) determines the usual unitary system evolution under the action of the system Hamiltonian $\hat{H}_\mathrm{S}$. Although the SSE employs the system Hilbert space only, the coupling to the bath is still included by the second term that describes dissipation effects due to the system-bath interaction. Finally, the third term introduces fluctuations in the time evolution: Although the dissipative term causes the probability density to decay in time, the norm of the state vector $\Psi(t)$ averaged over a statistical ensemble of realizations is conserved up to fourth order in the system-bath coupling parameter λ. In the following, we focus on a single bath operator $\hat{S}$ and, for the sake of clarity of our notation, omit indices at the bath operator.

As a result of the stochastic nature of Eq. (4), the system wave function can not be simulated by a single evolution of the SSE but needs to be represented by a statistical ensemble of wave functions $\{\Psi_s(t)\}$. Accordingly, starting from a pure initial state, the full time evolution of expectation values

$$\overline{O_\mathrm{S}}(t) = \overline{\langle \hat{O}_\mathrm{S} \rangle} = \overline{\langle \Psi(t)|\hat{O}_\mathrm{S}|\Psi(t)\rangle} \quad (6)$$

of physical observables needs to be calculated from the statistical average over all ensemble members as indicated by the bar. A reliable computation of smooth observables requires a large enough set of stochastic realizations.

B. Stochastic Schrödinger equation and Kohn-Sham density functional theory

So far, the complexity of solving the entire system Hamiltonian has been reduced via the SSE framework. Yet, still the question about the choice of bath operators and potential difficulties with describing the core system part remain. We address the question of appropriate electronic-structure theory methods for $\hat{H}_\mathrm{S}$ in this section before we turn to bath operators in the subsequent section.

The open quantum-system SSE approach has recently been extended [50, 51] to the framework of TD current density functional theory (TDCDFT) and its applicability has been discussed [53–55]. In contrast to standard TD(C)DFT, the open quantum-system approach operates on ensemble-averaged quantities. It requires the ensemble-averaged particle density

$$\overline{n(\mathbf{r},t)} = \overline{\langle \hat{n}(\mathbf{r}) \rangle}, \quad (7)$$

where the density operator is defined as

$$\hat{n}(\mathbf{r}) = \sum_i \delta(\mathbf{r} - \hat{\mathbf{r}}_i), \quad (8)$$

and the ensemble-averaged current density

$$\overline{\mathbf{j}(\mathbf{r},t)} = \overline{\langle \hat{\mathbf{j}}(\mathbf{r},t) \rangle}, \quad (9)$$

where the current operator reads

$$\hat{\mathbf{j}}(\mathbf{r},t) = \frac{1}{2}\sum_i \left\{ \delta(\mathbf{r} - \hat{\mathbf{r}}_i), \frac{\hat{\mathbf{p}}_i + \hat{\mathbf{A}}_\mathrm{ext}(\hat{\mathbf{r}}_i,t)}{m} \right\} \quad (10)$$

and $\{.,.\}$ denotes the anticommutator bracket. The theorem of stochastic TDCDFT of Refs. [50, 51] states that under reasonable physical conditions for a given and fixed bath operator $\hat{S}$, many-particle interaction $\hat{W}$, and initial state $\Psi(\mathbf{r}, t = 0)$, a one-to-one correspondence between the external vector potential $\mathbf{A}_\mathrm{ext}(\mathbf{r},t)$ and the ensemble-averaged current density $\overline{\mathbf{j}(\mathbf{r},t)}$ exists. Thus, the theorem paves the way for a non-interacting KS scheme of open quantum-system TDCDFT as it guarantees the uniqueness of a KS system that yields the same current density as the true interacting system. The corresponding KS Hamiltonian reads

$$\begin{aligned}\hat{H}_\mathrm{KS} = \sum_i \Bigg[& \frac{[\hat{\mathbf{p}}_i + \hat{\mathbf{A}}_\mathrm{ext}(\hat{\mathbf{r}}_i,t) + \hat{\mathbf{A}}_\mathrm{xc}(\hat{\mathbf{r}}_i,t)]^2}{2} \\ & + \hat{v}_\mathrm{ext}(\hat{\mathbf{r}}_i,t) + \hat{v}_\mathrm{H}(\hat{\mathbf{r}}_i,t) \Bigg],\end{aligned} \quad (11)$$

with the xc vector potential $\mathbf{A}_\mathrm{xc}(\mathbf{r},t)$ and the Hartree potential $v_\mathrm{H}(\mathbf{r},t)$. The xc vector potential in the open quantum-system approach may in general depend on $\overline{\mathbf{j}(\mathbf{r},t)}$, the initial state $\Phi_\mathrm{KS}(\mathbf{r}, t = 0)$, and the bath operator $\hat{S}$. The system dynamics can be calculated from the KS Slater determinant $\Phi_\mathrm{KS}(\mathbf{r},t)$ evolving according to the open system KS equation [50]

$$ß\partial_t \Phi_\mathrm{KS}(t) = \hat{H}_\mathrm{KS}\Phi_\mathrm{KS}(t) - \frac{ß}{2}\hat{S}^\dagger\hat{S}\Phi_\mathrm{KS}(t) + l(t)\hat{S}\Phi_\mathrm{KS}(t). \quad (12)$$

For practical calculations however, one needs to rely on existing approximations for the xc vector potential as the true $\mathbf{A}_\mathrm{xc}(\mathbf{r},t)$, especially in open quantum systems, is not known [50].

The ensemble-averaged current density – the basic property of the stochastic TDCDFT framework – is related to the ensemble-averaged density via the continuity equation of the open quantum system [51, 71]

$$\partial_t \overline{n(\mathbf{r},t)} = -\nabla \overline{\mathbf{j}(\mathbf{r},t)} + \mathcal{F}_\mathrm{B}(\mathbf{r},t). \quad (13)$$

The density modulation that is induced by the bath is described by

$$\mathcal{F}_\mathrm{B}(\mathbf{r},t) = \frac{1}{2}\overline{\langle 2\hat{S}^\dagger\hat{n}(\mathbf{r},t)\hat{S} - \hat{S}^\dagger\hat{S}\hat{n}(\mathbf{r},t) - \hat{n}(\mathbf{r},t)\hat{S}^\dagger\hat{S} \rangle}. \quad (14)$$

The proof of the above stated one-to-one correspondence requires implicitly that $\mathcal{F}_{\mathrm{B}}(\mathbf{r},t)$ is a functional of $\overline{n(\mathbf{r},t)}$ and $\overline{\mathbf{j}(\mathbf{r},t)}$ alone and can be solved uniquely to determine $\overline{n(\mathbf{r},t)}$ [53, 59]. However, although there is a unique relation between the density and the current density, the proof guarantees only the one-to-one correspondence between $\overline{\mathbf{j}(\mathbf{r},t)}$ and the vector potential. The ensemble-averaged density of the true and the non-interacting system are not necessarily equal. Therefore, the proof cannot be extended straight forwardly to a stochastic TDDFT framework where a one-to-one correspondence of the scalar potential $v_{\mathrm{ext}}(\mathbf{r},t)$ and $\overline{n(\mathbf{r},t)}$ would be needed to set up a non-interacting density-based TDDFT KS Hamiltonian. Yet, for applications that are based on the time evolution of the density such as the following ones, it is of great interest to find an open quantum-system approach in the framework of TDDFT.

Extensions of TDDFT to open quantum systems were already performed by Burke *et al.* [49] and Yuen-Zhou *et al.* [60] based on density matrices and master equations. Both strategies aim at the representation of the density of the interacting open quantum system by an auxiliary system with a different particle-particle interaction. To prove the validity of such approaches, one needs to find the corresponding external potential of the auxiliary KS system that produces the same density under given conditions. The proofs of Refs. [49] and [60] are based on the reasoning of Refs. [36, 72, 73] and rely on assumptions about the action of the bath operator. Yet, details about the consequences of these assumptions, in particular with regard to practical calculations and choices of the bath operator, are open questions in the field, and the use of approximate KS Hamiltonians in master equations and related implications have not been fully explored. A conclusive extension of the proof of stochastic TDCDFT that abandons the ensemble-averaged current density and establishes an open quantum-system TDDFT scheme based on the ensemble-averaged density alone is not available yet.

Therefore, practical applications of stochastic TDDFT so far rely on approximate realizations of the stochastic formalism in KS TDDFT. In the approach of Refs. [52, 53], the system Hamiltonian is approximated by a standard TDDFT Hamiltonian

$$\hat{H}_{\mathrm{KS}} = \sum_i \underbrace{\left[-\frac{\hat{\nabla}_i^2}{2} + \hat{v}_{\mathrm{ext}}(\hat{\mathbf{r}}_i,t) + \hat{v}_{\mathrm{H}}(\hat{\mathbf{r}}_i,t) + \hat{v}_{\mathrm{xc}}(\hat{\mathbf{r}}_i,t) \right]}_{=:\hat{h}_{\mathrm{KS}}(\hat{\mathbf{r}}_i,t)} \tag{15}$$

and used in the open quantum-system KS equation (12) together with a heuristic bath operator [57]. Here, we apply an open quantum-system KS scheme of the same kind and treat xc effects on the level of the adiabatic local density approximation. More background about the difficulty of establishing a DFT Hamiltonian in the open quantum-system framework, as for instance about issues like the v-representability problem of the current density [74], is provided elsewhere [75].

C. Bath operators in stochastic time-dependent density functional theory

The choice of the bath operator is the second ingredient for defining the open quantum-system scheme. Here, we apply a bath operator that introduces dissipation of the excited quantum system back to its ground state. The operator is a projector that reads

$$\hat{S} = \sqrt{\gamma} M[n(\mathbf{r},t)] |\Phi_{\mathrm{KS}}(t_0)\rangle\langle\Phi_{\mathrm{KS}}(t)|. \tag{16}$$

It exhibits the scaling factors $\sqrt{\gamma}$ and $M[n(\mathbf{r},t)]$. Choosing $M = 1$ amounts to a deexcitation of the entire system with decay rate γ and decay time constant $\tau = 1/\gamma$. The bath operator (16) covers a broader range of physical applications if one chooses a density-dependent factor $M[n(\mathbf{r},t)]$ that renders the operator sensitive to moments of the density. For physical processes, as for instance absorption and emission, it is interesting to consider a dissipation mechanism that depends on the (transition) dipole moment of the excited system. Such a coupling to the dipole moment can be obtained by choosing M proportional to the time variation of the dipole moment $\mathbf{d}(t) = \int \mathbf{r} n(\mathbf{r},t)\, \mathrm{d}^3r$, i.e., $M[n(\mathbf{r},t)] \propto |\mathbf{d}(t) - \mathbf{d}(t_0)|$. In the same way, a coupling to other moments of the density, as for instance particle-number, dipole-moment, or quadrupole-moment fluctuations, can be introduced via M. Note, that we model only the system part of the system-bath interaction as the bath side of the coupling mechanism is subsumed in the effective decay rate.

D. Simulation algorithm

Having introduced the stochastic TDDFT formalism and having discussed physically interesting bath operators, we finally turn our attention to the practical algorithm that we used to solve the open system KS equations. Our simulations are conducted with the quantum-jump algorithm [65, 67, 76, 77] that has been introduced in the context of open quantum-system KS equations in Ref. [53]. The algorithm is implemented in the Bayreuth version [78, 79] of the PARSEC program package [80] and rests upon the single-particle bath operator

$$\hat{s}_i = \sqrt{\gamma} M[n(\mathbf{r},t)] |\varphi_i(t_0)\rangle\langle\varphi_i(t)|. \tag{17}$$

We demonstrate in Appendix A that using this bath operator in the following set of quantum-jump single-particle equations is equivalent to using $\hat{S}$ in the corresponding algorithm for solving Eq. (12). The quantum-jump algorithm relies on a piecewise deterministic evolution [67] of the set of norm-preserving Schrödinger equations

$$ß\partial_t \varphi_i(t) = \hat{h}_{\mathrm{KS}} \varphi_i(t) - \frac{ß}{2} \hat{s}_i^\dagger \hat{s}_i \varphi_i(t) + \frac{ß}{2} |\hat{s}_i \varphi_i(t)|^2 \varphi_i(t), \tag{18}$$

that are interrupted by quantum jumps. The quantum jumps represent the non-deterministic action of the bath operator. The points of time where such a jump occurs are determined by a random process according to a waiting-time distribution. However, as this waiting-time distribution is not known beforehand, it needs to be determined alongside the actual propagation of the open quantum KS system (for details, see Ref. [53]): The waiting-time distribution can be determined from the decay of the norm

$$\eta(t) = \frac{1}{N} \sum_i \int |\varphi_i^{\mathrm{aux}}(\mathbf{r}, t)|^2 \, \mathrm{d}^3 r \tag{19}$$

of an auxiliary system of N particles in contact with the bath evolving according to

$$ß\partial_t \varphi_i^{\mathrm{aux}}(t) = \hat{h}_{\mathrm{KS}} \varphi_i^{\mathrm{aux}}(t) - \frac{ß}{2} \hat{s}_i^\dagger \hat{s}_i \varphi_i^{\mathrm{aux}}(t). \tag{20}$$

In this system, norm conservation is not build in explicitly. One obtains single waiting times by drawing random numbers in the interval [0,1] and choosing the time T when $\eta(T)$ drops below this number as the quantum-jump time. The waiting-time distribution can be calculated from many samples of such single jump times.

Due to the special choice of the bath operator that we consider in this work, some practical advantages occur in the algorithm: As the bath mechanism relaxes the system to its ground state and if no additional external perturbations act after the initial excitation, the system remains in the ground state after each quantum jump. As a consequence of this model bath interaction, the time evolutions of all orbitals of the stochastic ensemble follow the same pattern: The KS system evolves deterministically until a quantum jump occurs. Then, back in the ground state, the system propagates trivially with TD phases according to the KS eigenvalues as the bath operator does not act on the ground state. Therefore, the full statistical ensemble can be generated from a single deterministic evolution of Eq. (18) alongside with the determination of the waiting-time distribution: (i) calculate a long enough deterministic evolution together with the norm decay of the auxiliary system, (ii) draw a large number of random numbers, find the corresponding quantum-jump times, and determine the waiting-time distribution, (iii) generate single trajectories of the ensemble where the time evolution up to the jump is determined by the deterministic evolution and ground-state values are used for the time after the jump. The physical quantities of interest follow from averaging over corresponding observables according to Eq. (6) calculated from the thus obtained statistical ensemble. Moreover, the bath operator preserves the orthogonality of the KS orbitals and, therefore, an explicit orthogonalization of the orbitals as it is performed in Ref. [53] is not needed in the present scheme.

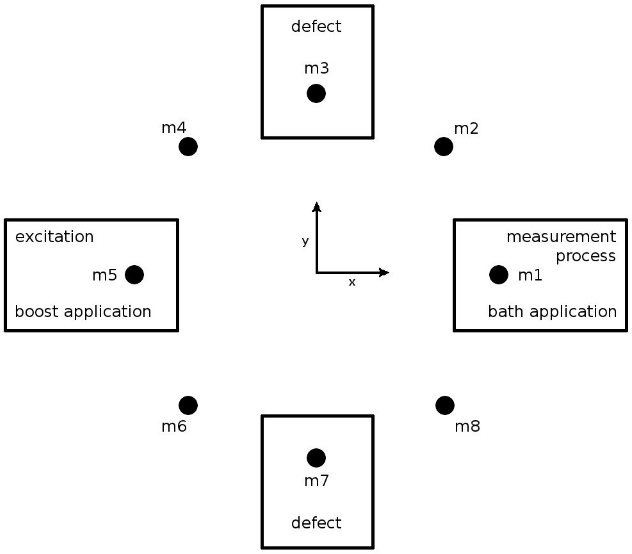

FIG. 1. Illustration of the model setup which is a circular arrangement of eight molecules m1, m2, ..., m8 with equal distances between all molecules. The excitation of the entire ring setup is performed via a localized momentum boost in the region of molecule m5. We measure the excitation spread in this arrangement by application of a dissipative bath operator in terms of a measurement process at molecule m1. For a transparent investigation of the influence of the intermolecular coupling and the energetic arrangement of the molecules on energy-transfer pathways, we introduce defects in the molecules m3 and m7. All other molecules are fixed according to their ground-state geometry, but their electronic state is allowed to evolve in time. (See Appendix B for more details about the specific setup used in Sec. IV.)

III. MODEL SYSTEM AND BATH COUPLING MECHANISM

A. Model setup

Having established the conceptual details of our approach, we turn to practical applications. In the following, we deal with a model system of circularly arranged molecules that is designed in the style of circular LH complexes of the antenna system of LH organisms (see Fig. 1). Our aim is to study the influence of electronic-structure properties on the EET time scale and pathways in such supermolecules. Here, we focus on the influence of the coupling and the energetic arrangement. With this in mind, the physical picture behind our calculations is the following: One molecule of the complex is excited due to light absorption. Then, the excitation travels in the system where the transfer mechanism is coherent EET via the electronic degrees of freedom. As a result the entire complex gets excited and we intend to measure the time scale of this excitation spread.

In our basic model setup consisting of eight molecules as indicated in Fig. 1, all molecules in the circular arrangement and all intermolecular distances are equal.

Initially, starting from the ground state of the setup we introduce an excitation at one of the molecules. To be explicit in our assignment, we take molecule m5. We simulate the excitation due to light absorption by a momentum boost. In practical calculations, this boost is applied only in one section of the real-space grid, so that only molecule m5 gets excited.

The bath operator plays the role of a measurement process that determines the time an initial excitation travels within the ring system. In our setup, it operates on molecule m1 on the opposite side of the initial excitation to measure the time scale the excitation needs to travel halfway through the ring. The measurement process is supposed to model deexcitation, thus remove the entire excitation energy out of the system when the initial excitation has reached molecule m1. In contrast to true molecules where typically due to relaxation the excitation moves to lower lying energy levels, here the measurement processes immediately brings the supermolecule back to its ground state. It is an incoherent mechanism without back transfer from the bath to the system. We assume that the bath is sensitive to dipolar excitations and couples to the dipole moment of molecule m1. For these reasons, we take the bath mechanism introduced in Eq. (16) in its single-particle version of Eq. (17) and design it to be sensitive to dipolar excitations: It detects changes of the dipole moment $|\mathbf{d}_1(t)-\mathbf{d}_1(t_0)|$ of molecule m1 only. Here, the index denotes molecule m1 and indicates that the dipole moment is calculated only in the corresponding section of the grid. The corresponding scaling factor M of the bath operator includes a normalization factor D and reads

$$M[n(\mathbf{r},t)] = \frac{|\mathbf{d}_1(t) - \mathbf{d}_1(t_0)|}{D}. \tag{21}$$

In this approach, the time constant related to the rate of the dissipative mechanism is a free parameter, whereas D needs to be chosen reasonably as discussed in Sec. III B. In summary, the bath mechanism measures locally how much of the excitation energy has reached molecule m1 and deexcites the entire system accordingly.

For a transparent analysis of the influence of the coupling mechanism and the energetic arrangement, we choose dimers to be the components of the circular system (see Appendix B). In dimers, the electronic structure can be modified easily by bond-length variation. Thus, it is straight forward to introduce defects in terms of modifications of the electronic structure as indicated in Fig. 1. To guarantee uniqueness and transparency of our investigations in Sec. IV, we modify only molecules m3 and m7, and fix all other system components. The electronic-structure properties of the model system are discussed in detail in Appendix B. However, the following considerations are not restricted to dimers but can be applied to more general systems. In a circular arrangement of model molecules, there are at least three time scales relevant for the signal observed on the ring: the time scale related to the energy of the excited states, the time scale due to intermolecular coupling (here, more time scales are involved if the system is partly or in total off-resonant), and the time scale due to dissipative bath action. The influence of the bath mechanism on a single dimer is discussed in the following before we present our results on the life time of the excitation on the ring in Sec. IV.

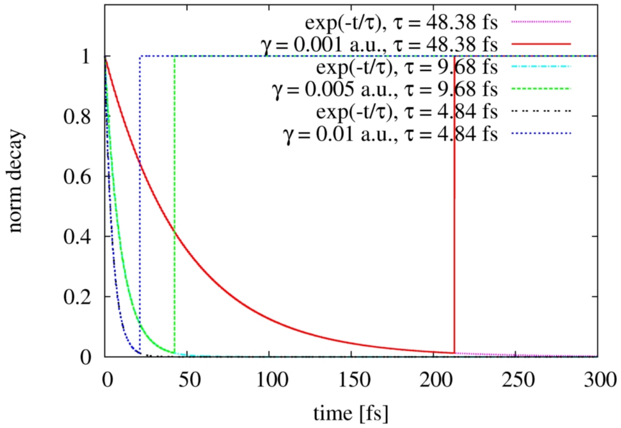

FIG. 2. Norm decay $\eta(t)$ of a single model molecule. The damping is performed with different decay-time constants τ after an initial boost excitation with 0.001 eV excitation energy. The norm decay always follows an exponential function $\exp(-t/\tau)$ with the preset time τ. Here, quantum jumps were performed as the norm dropped below 0.014 %. They manifest in vertical lines where the norm jumps back to one and stays for the rest of the time evolution as the bath operator does not act on the ground state.

B. Assessment of the bath operator

In this section, we discuss the behaviour of our model bath operator, i.e., we adjust the normalization factor D of Eq. (21) and investigate the effect of the bath operator on a single molecule. The aim of this investigation is to find D such that the functionality of the scaling factors γ and $(|\mathbf{d}_1(t)-\mathbf{d}_1(t_0)|)/D$ in front of the projector is clearly split into two contributions: D needs to be determined such that the decay time τ of the relaxation process is determined only by the decay rate γ, thus $\tau = 1/\gamma$. The dipole dependent scaling factor is intended to account for the coupling to the dipole moment of molecule m1 and should not interfere with the role of γ. Therefore, D needs to be adapted to the dipole oscillations of the isolated model molecule m1. In the following, we outline a procedure for the determination of D and investigate some relevant influencing factors.

To determine D, we calculated 100 fs of the dipole-moment time evolution of a single molecule in a closed quantum system after an initial momentum boost. We apply the momentum boost along the bond axis of the dimer. Thus, only the dipole moment along this axis gets excited and the investigation can be restricted to

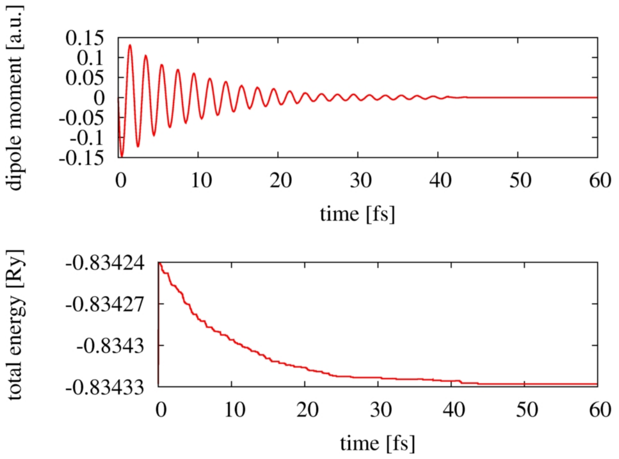

FIG. 3. Ensemble-averaged dipole moment (z-component) and total energy of a single molecule in contact with a dissipative bath that induces a decay time of 10 fs.

this dipole-moment component. There are various different options to compute D based on the existing dipole-moment data: It may be chosen to be e.g. the first maximum, the average over all maxima, the absolute average, or the absolute square average of the dipole moment. We find by numerical tests that only normalization according to the average of the absolute square of the dipole moment gives an exponential decay with time constant τ that we aimed at by setting the decay rate. Moreover, we checked this observation with different decay-time constants in Fig. 2 where we plotted the norm decay of the auxiliary system of the quantum-jump algorithm. All computed decay times complied with the preset decay rate.

Another influencing factor on the determination of D is the energy that we introduce into the system by the boost excitation. We interpret the excitation procedure as a single absorption process of an energy portion. The dissipation of such an energy portion due to the measurement process should be independent of the boost strength as long as the boost strength corresponds to a single excitation process. Therefore, in the single excitation case, the normalization factor needs to be adapted to the boost strength. We guarantee for the boost strength adaptation by always determining D from a closed quantum-system calculation with the same initial boost excitation as in the open quantum-system calculation we aim at. We find that the thus obtained normalization factor yields a decay time that is independent of the boost strength.

The excitation process could likewise be performed by application of an external laser field. In this case, an instantaneous excitation could be simulated by a short pulse and the determination of the normalization factor should then be performed using the dipole signal after the pulse excitation.

Having investigated the norm decay in detail, we finally give some results on other important observables. The exponential decay of the norm translates into an exponential decay of the total energy and the envelope of the dipole-moment oscillation (see Fig. 3). Thus, the bath operator fulfills all desired criteria and is ready for application in more complex molecular systems.

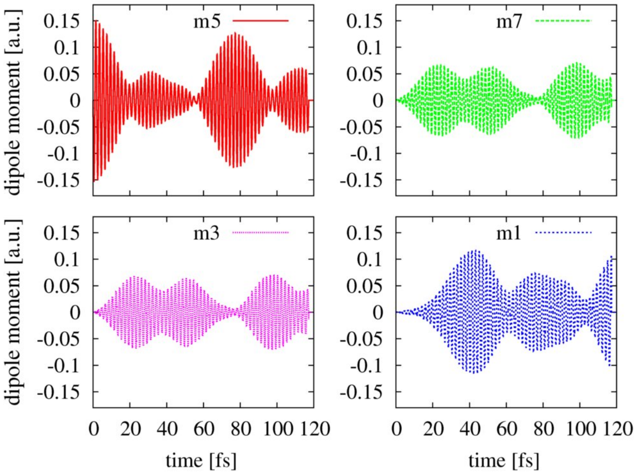

FIG. 4. Coherent time evolution of the dipole moment (z-component) of four molecules of a circular setup of eight identical molecules arranged according to Fig. 1. The intermolecular distance is 20 bohr. Here, an initial boost excitation was applied at $t = 0$ in the subsystem m5 and no dissipative mechanism acts within the entire system. The oscillation pattern emerges due to interference of the dipolar excitation that is traveling in the ring system along both directions.

IV. RESULTS AND DISCUSSION

A. Resonant excitation spread and decay time constants

As a first step towards the investigation of EET in circular supermolecules, we study the perfectly resonant coupling situation where all molecules are the same. We start with the fully coherent case without system-bath coupling. Apart from this, we take the setup of Fig. 1 with an intermolecular distance of 20 bohr and perform the boost excitation at molecule m5 as explained in Sec. III. The time evolution of the dipole moment of four molecules of this ring configuration is depicted in Fig. 4. We observe a fast oscillation of the dipole moment that corresponds to the lowest excitation energy of our model system at 2.1 eV while the envelope follows an interference pattern: At different points of time the largest dipole moment amplitude can be observed at different subsystems. This interference pattern emerges as the dipolar excitation travels in the ring system along both directions. It is governed by the intermolecular coupling strength, i.e., the pattern is determined by time an excitation needs to be transferred between neighboring molecules. In our model system at a separation of 20 bohr the coupling strength is 0.038 eV [81]. If two of

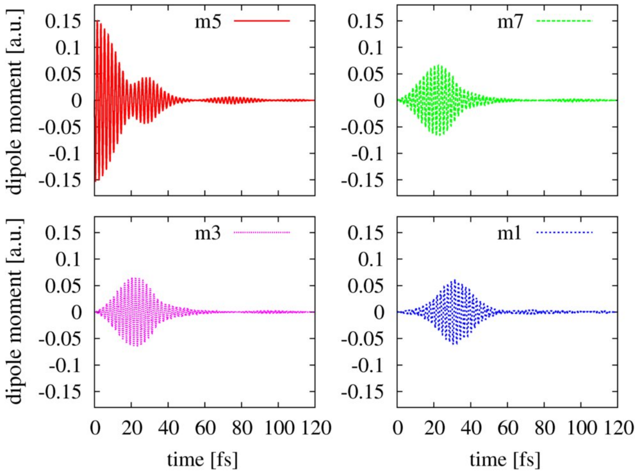

FIG. 5. Ensemble-averaged dipole moment (z-component) time evolution of four molecules that are arranged as in Fig. 4. After the initial boost excitation at molecule m5, the excitation travels in the ring and decays due to a dissipative bath that is acting with a decay time of 5 fs on molecule m1.

those model molecules were isolated, this would amount to a resonance oscillation with a cycle duration of 107.8 fs. In this case, after each quarter of this period the maximum of the dipole oscillation can be observed on one of the two neighbors [81]. Yet back in the circular setup, each molecule has neighbors on both sides, thus provides a pathway for excitation spread.

We now add the bath mechanism of Sec. III acting on molecule m1. To measure the EET time, the bath needs to break the interference of the so far fully coherent energy spread, thus it needs to operate on a comparably short time scale. Here, it acts with a decay time of 5 fs. This choice will be motivated further in the following. Again, we depict in Fig. 5 the time evolution of the dipole moment of the same four molecules. Due to the bath mechanism, an additional time scale comes into play and one observes clearly how the oscillation of the dipole moment decays in all subsystems of the ring due to the dissipative process. The coupling to the bath breaks the coherent evolution and causes relaxation of the system back to its ground state. To be able to measure the traveling time of an excitation in the circular setup, the decay time needs to be chosen short enough to sample the initial stage of the coherent EET before the interference pattern starts to build up. In the example of Fig. 5, the decay time of 5 fs fulfills this criterion: The dipole oscillation at molecule m1 reaches only one maximum and subsequently decays to the ground state, thus no interference emerges.

In this open quantum-system simulation, the decay of the norm $\eta(T)$ of the auxiliary system indicates how much of the excitation energy has reached molecule m1. Therefore, it serves as a measure for the life time of the excitation on the ring traveling from molecule m5 to molecule m1 before relaxation occurs. We monitor $\eta(T)$ and take the times T when $\eta(T)$ drops below preset thresholds to quantify this life time. However, due to the interference along the excitation spread, monitoring just a single threshold of this norm decay may be dominated by interference effects, thus its meaningfulness may be compromised. Therefore, we considered the norm decay down to three different thresholds: 0.100, 0.050, and 0.012. The times T for the perfectly resonant situation are listed in Table I. They serve as a starting point for investigating the influence of electronic-structure properties on the time an excitation needs to spread in the circular arrangement of the model system with an intermolecular distance of 20 bohr.

m3	m7	$\eta = 0.100$	$\eta = 0.050$	$\eta = 0.012$
0.0 bohr	0.0 bohr	52 fs	75 fs	117 fs
-0.1 bohr	0.0 bohr	56 fs	110 fs	121 fs
-0.5 bohr	0.0 bohr	84 fs	97 fs	143 fs
-0.1 bohr	-0.1 bohr	57 fs	112 fs	123 fs
-0.1 bohr	-0.5 bohr	85 fs	97 fs	157 fs
-0.5 bohr	-0.5 bohr	166 fs	181 fs	211 fs
removed	0.0 bohr	80 fs	89 fs	125 fs
removed	-0.1 bohr	99 fs	125 fs	147 fs
removed	-0.5 bohr	205 fs	227 fs	265 fs

TABLE I. Times T where the norm $\eta(T)$ of the decaying auxiliary system drops below 0.100, 0.050, and 0.012 for different modifications of the molecular arrangement. The calculations are performed in a circular setup of model molecules (see Fig. 1) with an intermolecular distance of 20 bohr. We modified the electronic structure by systematically introducing defects in the molecules m3 and m7 in terms of bond-length variation and/or removing one of the molecules. These modifications are indicated in the first two columns of the table. In our model system, a bond-length reduction of 0.1 bohr (0.5 bohr) amounts to an energetic detuning of the excitation energy by 0.049 eV (0.135 eV) and a reduction of the coupling-matrix element by 0.006 eV (0.012 eV).

B. Influence of energetic disorder

Having examined the resonant excitation-energy spread, we now assess the influence of energetic disorder on the EET time scales by introducing defects in the ring setup. Such defects can be inserted via bond-length variations and/or removing one of the molecules. We compare in Table I the times T to the fully resonant situation of the previous section. We find that small changes of the bond length of -0.1 bohr in molecule m3 or in both molecules m3 and m7 result in a minor increase of the time scale set by the resonant case. Larger increases of the time T can be observed in cases where in one of the molecules the bond length was changed by -0.5 bohr. Note, that already in the data set discussed so far the influence of interference effects on the life times of the excitation on the ring can be observed: While the times corresponding to the decay down to $\eta = 0.100$ and $\eta = 0.012$ give a clear picture, the times T at $\eta = 0.050$ exhibit a different behavior. Yet, we observe a clear rise of the transfer time as soon as the more severe defect of -0.5 bohr bond-length variation was introduced in both pathways between the initially excited molecule and the molecule where the measurement process works. The increase of this life time of the excitation on the ring is on the order of a factor of two.

As another defect, we investigated a setup where molecule m3 was removed from the ring. In this case, the coupling between molecules m2 and m4 is smaller by about an order of magnitude than the previous coupling strength between m3 and its neighbors [81]. In this situation, as long as all other molecules are perfectly resonant, the times T increase due to less severe defects in molecule m3 by about the same amount as before. Introducing additional defects in molecule m7, the energy-transfer process slows down notably as we observe the longest times T in case of removed molecule m3 and bond-length variation of -0.5 bohr in molecule m7.

In conclusion, we find that in cases of resonance or close to resonance the EET time scale is not affected much by variations of the coupling strength and interference effects play a role for the life time of the excitation on the ring corresponding to specific setups. However, as soon as sizable defects occur in both pathways of energy transfer, the time scales determined by our measurement process notably increase, thus EET is hindered noticeably.

C. Influence of the intrasystem coupling

In the final investigation, we examine the influence of the intermolecular electronic-coupling mechanism on the life time of the excitation on the ring. Here, we focus on the difference between full electronic coupling and the dipole-dipole coupling that is performed in the prominent Förster theory of EET [81–83]. In order to observe noticeable differences between Förster-type and full coupling, we had to go to an intermolecular distance regime where such differences occur. For our model system, it is known that significant differences from the dipole-dipole coupling can be observed for distances below 20 bohr where the dipole-dipole coupling approximation overestimates the true coupling strength [81]. Therefore, we switched to a circular setup of 12 bohr distance between the molecules to guarantee for a clear analysis of the influence of the coupling behavior. We decided to keep the dissipation time constant of 5 fs of our previous calculations although for 12 bohr intermolecular distance the coupling-matrix element of 0.105 eV is notably larger than in the previous case [81]. Our results are compiled in Table II.

coupling	m3	$\eta = 0.100$	$\eta = 0.050$	$\eta = 0.012$
full	0.0 bohr	95 fs	116 fs	163 fs
Förster	0.0 bohr	86 fs	104 fs	152 fs
full	-0.1 bohr	99 fs	140 fs	182 fs
Förster	-0.1 bohr	94 fs	108 fs	154 fs
full	-0.5 bohr	109 fs	140 fs	209 fs
Förster	-0.5 bohr	89 fs	115 fs	185 fs

TABLE II. Investigation of the times T where $\eta(T)$ drops below the thresholds of 0.100, 0.050, and 0.012. The molecules are arranged at a distance of 12 bohr. Thus, notable differences of the coupling strength exist between the cases of full electronic coupling and Förster-type dipole-dipole coupling [81]. Moreover, defects in terms of bond-length variation are introduced in molecule m3 as indicated in the second column.

We find that Förster-type coupling overestimates the times T determined by the measurement process in comparison to the true electronic coupling, thus it overestimates EET in the setup. This finding parallels the fact that also the coupling-matrix element is overestimated by the dipole-dipole coupling [81]. This result was consistently confirmed also in situations where defects were introduced in the circular arrangement. Finally, we note that the times T observed for an intermolecular distance of 12 bohr are smaller than the numbers for 20 bohr, although in the latter case the coupling is notably weaker. This finding comes as a result of interference effects that are more pronounced in cases of stronger coupling. Therefore, it is difficult to compare absolute time scales unless the dissipation time constant of the measurement process is chosen short enough to prevent a buildup of interference due to excitation-energy spread along different available pathways.

V. SUMMARY AND CONCLUSIONS

In summary, we used an open quantum-system scheme in the framework of TDDFT to investigate the excitation-energy spread in a circular arrangement of molecules in the spirit of LH complexes. To this end, we introduced a bath mechanism that couples to the dipole moment of specific subsystems of the supermolecular complex and operates in terms of a measurement process. We find that this dissipative mechanism breaks the interference pattern of coherent EET and removes excitation energy from the system. The time scale of this relaxation is determined by the intermolecular coupling and the dissipation time constant. In this context, it is the strength of (TD)DFT to be accurate on the level of available xc functional approximations in the determination of the electronic structure of the entire complex and its subsystems. Therefore, the influence of electronic-structure properties and intermolecular coupling mechanisms on the EET process can be investigated straight forwardly. Our results demonstrate that small deviations of the electronic structure, e.g. via bond-length variation, cause only minor changes of the time scale monitored by the measurement process. Only when all energy-transfer pathways in the circular setup suffer from sizable defects, the EET time drops notably. Similarly, variations of the coupling mechanism, as for example via Förster-type dipole-dipole coupling, change the EET times according to the changes of the coupling strength.

ACKNOWLEDGMENTS

Financial support by the Elitestudiengang Macromolecular Science, the DFG Graduiertenkolleg 1640, and the German-Israeli Foundation is gratefully acknowledged.

Appendix A: Single-particle representation of the bath operator

In this appendix, we demonstrate that using the single-particle operator $\hat{s}_i$ of Eq. (17) in the set of single-particle equations of Sec. II D is equivalent to solving Eq. (12) with the bath operator $\hat{S}$ of Eq. (16) using the quantum-jump algorithm. In the latter case, one needs to propagate simultaneously the norm-preserving equation

$$ß\partial_t \Phi_{\mathrm{KS}} = \hat{H}_{\mathrm{KS}}\Phi_{\mathrm{KS}} - \frac{ß}{2}\hat{S}^\dagger \hat{S}\Phi_{\mathrm{KS}} + \frac{ß}{2}||\hat{S}\Phi_{\mathrm{KS}}||^2\Phi_{\mathrm{KS}} \quad \text{(A1)}$$

and the auxiliary equation

$$ß\partial_t \Phi_{\mathrm{KS}}^{\mathrm{aux}} = \hat{H}_{\mathrm{KS}}\Phi_{\mathrm{KS}}^{\mathrm{aux}} - \frac{ß}{2}\hat{S}^\dagger \hat{S}\Phi_{\mathrm{KS}}^{\mathrm{aux}}. \quad \text{(A2)}$$

Inserting $\hat{S}$ of Eq. (16) in Eq. (A1) yields the closed quantum-system KS equation

$$ß\partial_t \Phi_{\mathrm{KS}} = \hat{H}_{\mathrm{KS}}\Phi_{\mathrm{KS}}. \quad \text{(A3)}$$

The latter equation can be translated to the well-known set of single-particle KS equations that one also obtains by inserting $\hat{s}_i$ of Eq. (17) into Eq. (18).

Therefore, it remains to be checked if, given our choice of bath operators, Eq. (A2) translated to a set of single-particle equations coincides with Eq. (20). To this end, we use the method of Ref. [84] to find the single-particle form of Eq. (A2). The method starts from the reduced one-body density matrix

$$\begin{aligned}\rho(\mathbf{r},\mathbf{r}',t) = \int &\Phi_{\mathrm{KS}}(\mathbf{r},\mathbf{r}_2,\dots,\mathbf{r}_N)\\ &\Phi_{\mathrm{KS}}^*(\mathbf{r}',\mathbf{r}_2,\dots,\mathbf{r}_N)\,\mathrm{d}^3r_2\dots\mathrm{d}^3r_N.\end{aligned} \quad \text{(A4)}$$

Computing the equation of motion of the one-body density matrix by inserting the open quantum-system KS equation and the specific choice of $\hat{S}$ of Eq. (16) yields

$$\begin{aligned}&ß\partial_t\rho(\mathbf{r},\mathbf{r}',t) =\\ &\left[\hat{h}_{\mathrm{KS}}(\mathbf{r},t) - \frac{ß}{2}\gamma M^2 - \left(\hat{h}_{\mathrm{KS}}(\mathbf{r}',t) + \frac{ß}{2}\gamma M^2\right)\right]\rho(\mathbf{r},\mathbf{r}',t).\end{aligned} \quad \text{(A5)}$$

Note, that M is defined in the context of Eq. (16). Next, we express $\rho(\mathbf{r},\mathbf{r}',t)$ in terms of a representation of N orthonormal basis functions $\tilde{\varphi}_j$ [84] according to

$$\rho(\mathbf{r},\mathbf{r}',t) = \sum_{j=1}^{N}\tilde{\varphi}_j(\mathbf{r},t)\tilde{\varphi}_j^*(\mathbf{r}',t). \quad \text{(A6)}$$

Applying this representation to Eq. (A5) yields for the case without dissipation ($\gamma = 0$)

$$\begin{aligned}&\sum_{j=1}^{N}\tilde{\varphi}_j^*(\mathbf{r}',t)\left[ß\partial_t - \hat{h}_{\mathrm{KS}}(\mathbf{r},t)\right]\tilde{\varphi}_j(\mathbf{r},t) =\\ &\sum_{j=1}^{N}\left\{\tilde{\varphi}_j^*(\mathbf{r},t)\left[ß\partial_t - \hat{h}_{\mathrm{KS}}(\mathbf{r}',t)\right]\tilde{\varphi}_j(\mathbf{r}',t)\right\}^*.\end{aligned} \quad \text{(A7)}$$

For the limit $\gamma = 0$, a single-particle representation can be obtained by introducing the time-dependent matrix

$$C_{jj'}(t) = \left\langle\tilde{\varphi}_j(t)\middle|ß\partial_t - \hat{h}_{\mathrm{KS}}(\mathbf{r},t)\middle|\tilde{\varphi}_{j'}(t)\right\rangle. \quad \text{(A8)}$$

Equation (A7) demonstrates that the matrix $C_{jj'}(t)$ is Hermitian (see also Ref. [84]) and, therefore, can be diagonalized. Based on this finding, we assume that $\{\tilde{\varphi}_j(\mathbf{r},t)\}$ is the diagonal basis, without loss of generality, and that it fulfills the eigenvalue equation

$$\left[ß\partial_t - \hat{h}_{\mathrm{KS}}(\mathbf{r},t)\right]\tilde{\varphi}_j(t) = \varepsilon_j(t)\tilde{\varphi}_j(t) \quad \text{(A9)}$$

with real-valued eigenvalues $\varepsilon_j(t)$. Next, we consider the case which includes dissipation. For $\gamma \neq 0$ we can introduce in a similar way a matrix $D_{jj'}(t)$ according to

$$\begin{aligned}D_{jj'}(t) &= \left\langle\tilde{\varphi}_j(t)\middle|ß\partial_t - \left(\hat{h}_{\mathrm{KS}}(\mathbf{r},t) - \frac{ß}{2}\gamma M^2\right)\middle|\tilde{\varphi}_{j'}(t)\right\rangle\\ &= C_{jj'}(t) + \frac{ß}{2}\gamma M^2\left\langle\tilde{\varphi}_j(t)|\tilde{\varphi}_{j'}(t)\right\rangle,\end{aligned} \quad \text{(A10)}$$

which includes the dissipative term. Note that $D_{jj'}(t)$ contains the Hermitian contribution $C_{jj'}(t)$ and an anti-Hermitian part $\frac{ß}{2}\gamma M^2\left\langle\tilde{\varphi}_j(t)|\tilde{\varphi}_{j'}(t)\right\rangle$. Since our dissipation operator is proportional to a unit operator, the matrix $D_{jj'}(t)$ also remains diagonal in the basis $\{\tilde{\varphi}_j(\mathbf{r},t)\}$. While the eigenvalues $\varepsilon_j(t)$ of $C_{jj'}(t)$ have been all real-valued, the eigenvalues $\epsilon_j(t)$ of $D_{jj'}(t)$ aquire a constant shift in the imaginary part

$$\epsilon_j(t) = \varepsilon_j(t) + \frac{ß}{2}\gamma M^2. \quad \text{(A11)}$$

Finally, we can set

$$\tilde{\varphi}_j(t) = \exp\left\{-ß\int_{t_0}^{t}\epsilon_j(\tau)\,\mathrm{d}\tau\right\}\varphi_j^{\mathrm{aux}}(t) \quad \text{(A12)}$$

to obtain the set of single-particle equations

$$ß\partial_t\varphi_j^{\mathrm{aux}}(t) = \hat{h}_{\mathrm{KS}}\varphi_j^{\mathrm{aux}}(t) - \frac{ß}{2}\gamma M^2\varphi_j^{\mathrm{aux}}(t). \quad \text{(A13)}$$

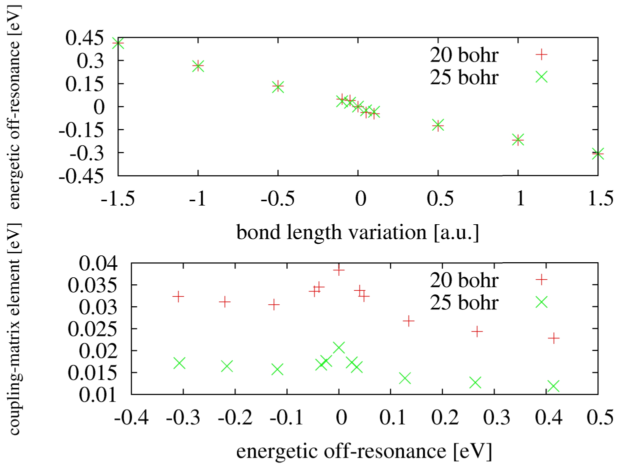

FIG. 6. Upper panel: Excitation-energy variation (energetic off-resonance) of one Na_2 depending on variations of the bond length. We computed this property from a supersystem calculation as explained in Appendix C using two different dimer distances. Lower panel: Coupling-matrix element calculated in a supersystem of two Na_2 depending on the energetic off-resonance of one of the dimers.

Note that due to the dissipation, the orbitals $\varphi_j^{\mathrm{aux}}(t)$ stay not normalized during the time-evolution.

To conclude, we have illustrated that the single particle equations in (A12) are equivalent to the set of equations (20) when the operator $\hat{s}_j$ is inserted. Therefore, the validity of the single-particle scheme for solving Eq. (12) with the bath operator $\hat{S}$ is established.

Appendix B: Details of the model system

To guarantee for a transparent analysis of the coupling and energetic arrangement, we choose sodium dimers as a well-approved model molecule [81, 85]. It exhibits strong dipolar character and the electronic structure can be modified easily by bond-length variation starting from the experimental bond length of 5.78 bohr. All sodium dimers are aligned along the z-axis according to the setup of Fig. 1 and their centers of mass are in the x-y-plane. In the following, we introduce the electronic-structure properties of our model system and investigate the intermolecular coupling situation.

1. Electronic structure of the subsystem

First, we discuss the electronic structure of one dimer and the influence of the bond length on the latter. We start with Na_2 at the experimental bond length. For excitations oriented along the bond axis, Na_2 is almost a single level atom as there is one prominent excitation at 2.1 eV and a second excitation at 4.1 eV with notably smaller oscillator strength. The changes of the excitation energy of the one prominent peak with variations of the bond length can be calculated along two different ways: either from straight forward TDDFT propagation of a dimer with shifted bond length or in a supersystem setup with two dimers where one of the dimer bond lengths is shifted (see Appendix C). We performed both methods and found reasonable agreement of the results shown in the upper panel of Fig. 6. We find that due to shifts of the bond length on the order of 1 bohr, excitation-energy fluctuations of about 0.25 eV can be induced.

2. Resonant and off-resonant coupling

Second, we consider the coupling between two neighboring molecules and therefore isolate a system of two Na_2. Here, we address two influencing factors, namely the distance between the dimers and the energetic arrangement determined by the dimer bond length. The distance dependence of the coupling-matrix element in a resonant situation with sodium dimers of equal bond length was already investigated in an earlier work [81]. This investigation was based on the Davydov splitting in a resonant two-level interpretation extracted from the dipole moment time evolution: For distances above 25 bohr, the coupling is of dipole-dipole type, whereas clear deviations from the dipole-dipole character can be observed for smaller distances.

In an off-resonant coupling situation between isolated excited states, a similar two-level picture [87] can be applied to determine the coupling-matrix element. In analogy to the resonant case, also in this situation, the coupling strength can be extracted from a suitable observation of the dipole moment of separate system parts (for details, see Appendix C). The results of the coupling-matrix element as a function of the energetic off-resonance of the excitation energy of one of the dimers are shown in the lower panel of Fig. 6. We find a general trend of the coupling-matrix element to decrease with increasing excitation energy within the data range investigated here. A clear resonance peak of the coupling strength appears at the resonant coupling situation. It is by about a factor of 1.4 larger than the coupling at off-resonant situations.

Appendix C: Off-resonant oscillation in the time-dependent dipole moment

In this appendix we briefly explain how the coupling strength and the energetic off-resonance in a system of one donor molecule D and one acceptor molecule A manifest in the TD dipole moment. Note, that the resonant coupling case was already discussed in Ref. [81]. Our considerations employ a two-state model [87] based on the assumption that the wave function of the total system can be separated into D and A parts due to negligible electronic coupling between D and A. Initially, the acceptor is in its ground state denoted by $|\mathrm{A}\rangle$ and the donor is in an excited state $|\mathrm{D}^*\rangle$. This amounts to an initial product state $|\mathrm{D}^*\mathrm{A}\rangle = |\mathrm{D}^*\rangle|\mathrm{A}\rangle = |1\rangle$. The final wave function corresponds to the inverse situation, where $|\mathrm{DA}^*\rangle = |2\rangle$. Both states are characterized by their eigenvalue E_1 and E_2. We measure possible energetic off-resonances by the parameter

$$\Delta E = \frac{1}{2}(E_1 - E_2). \tag{C1}$$

The coupling between $|1\rangle$ and $|2\rangle$ is mediated by the Coulomb interaction $\hat{V}_\mathrm{C}$. It leads to the coupling-matrix element

$$V = \langle \mathrm{DA}^*|\hat{V}_\mathrm{C}|\mathrm{D}^*\mathrm{A}\rangle. \tag{C2}$$

The time evolution of the two-state system with initial state $|\Psi(0)\rangle = |1\rangle$ is given by

$$|\Psi(t)\rangle = a_1(t)|1\rangle + a_2(t)|2\rangle \tag{C3}$$

with the coefficients $a_1(t)$ and $a_2(t)$ [88],

$$\begin{aligned} |a_1(t)|^2 &= B + A\cos^2\left(\sqrt{V^2+\Delta E^2}t\right), \\ |a_2(t)|^2 &= A\sin^2\left(\sqrt{V^2+\Delta E^2}t\right), \end{aligned} \tag{C4}$$

where $A = \frac{V^2}{V^2+\Delta E^2}$ and $B = \frac{\Delta E^2}{V^2+\Delta E^2}$. This time evolution of the coefficients corresponds to an incomplete oscillation with beat frequency $\omega_\mathrm{beat} = \sqrt{V^2+\Delta E^2}$ that depends on the coupling between the initial and the final state as well as the energetic off-resonance: The occupation probability of the initial state varies around B with amplitude A, while the occupation probability of the final state oscillates with amplitude A around zero.

The TD dipole moment $\mathbf{d}^\mathrm{A}(t) = \langle\Psi(t)|\hat{\mathbf{r}}^\mathrm{A}|\Psi(t)\rangle$ of the acceptor, where we take the dipole operator $\hat{\mathbf{r}}^\mathrm{A}$ in the space of the acceptor only, can be calculated as

$$\mathbf{d}^\mathrm{A}(t) = |a_1(t)|^2\langle\mathrm{A}|\hat{\mathbf{r}}^\mathrm{A}|\mathrm{A}\rangle + |a_2(t)|^2\langle\mathrm{A}^*|\hat{\mathbf{r}}^\mathrm{A}|\mathrm{A}^*\rangle. \tag{C5}$$

Here, we exploited the orthogonality of $|D\rangle$ and $|D^*\rangle$. If the static dipole moment $\langle A|\hat{\mathbf{r}}^\mathrm{A}|A\rangle$ of A vanishes, Eq. (C5) simplifies to

$$\mathbf{d}^\mathrm{A}(t) = |a_2(t)|^2\langle\mathrm{A}^*|\hat{\mathbf{r}}^\mathrm{A}|\mathrm{A}^*\rangle. \tag{C6}$$

Accordingly, with the assumption that the static donor dipole moment vanishes, the TD donor dipole moment reads

$$\mathbf{d}^\mathrm{D}(t) = |a_1(t)|^2\langle\mathrm{D}^*|\hat{\mathbf{r}}^\mathrm{D}|\mathrm{D}^*\rangle. \tag{C7}$$

Thus, the resonance oscillation of the coefficients can be observed in the time evolution of the dipole moments $\mathbf{d}^\mathrm{A}(t)$ and $\mathbf{d}^\mathrm{D}(t)$. In principle both Eqs. (C6) and (C7) can be used to determine the coupling-matrix element V. Of special importance is Eq. (C7) together with Eq. (C4) as a fit to the absolute of the extrema of the k-th component of the donor dipole moment time evolution provides Ap_k, Bp_k, and ω_beat, where $p_k = \langle\mathrm{D}^*|\hat{r}_k^\mathrm{D}|\mathrm{D}^*\rangle$. It can be used to determine V, ΔE, and p_k. One obtains

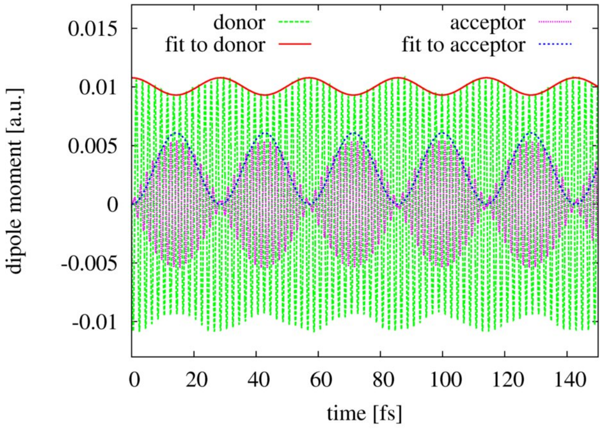

FIG. 7. Donor and acceptor dipole moment (z-component) in a setup of two Na_2, where the bond length of the acceptor Na_2 is reduced by 0.5 bohr compared to the experimental bond length. We performed fits to the envelope of the oscillation according to the model discussed in the text.

$$V = \sqrt{\frac{Ap_k}{Ap_k + Bp_k}}\omega_\mathrm{beat} \tag{C8}$$

and

$$\Delta E = \sqrt{\frac{Bp_k}{Ap_k + Bp_k}}\omega_\mathrm{beat}. \tag{C9}$$

A typical time evolution of the z-component of the acceptor and donor dipole moments of our model system is depicted in Fig. 7 together with our fits to the envelopes. Note, that the two-level model qualitatively fits to the dipole oscillation of the off-resonant, coupled system of two molecules. However, the dipole moment envelopes do not perfectly follow the $\sin^2$- and $\cos^2$-shape. We understand these deviations as a consequence of the coupled system not being perfectly separable into D and A parts as we assumed in the model. Furthermore, although the second excitation of Na_2 with polarization in z-direction is energetically far off and carries notably smaller oscillator strength, Na_2 is not a perfect single level system, and therefore the system of two sodium dimers does not perfectly fit into the two-level model. Nevertheless, our approach provides a tool to determine the coupling V and the energetic off-resonance ΔE. The validity of the model can be checked by comparison of the thus obtained ΔE to TDDFT excitation energies of single sodium dimers with shifted bond length. We find good agreement and, therefore, assume reasonable quality of the coupling-matrix element results of Fig. 6.

---

[1] W. Kühlbrandt, Nature **374**, 497 (1995).
[2] Y.-C. Cheng and G. R. Fleming, Annu. Rev. Phys. Chem. **60**, 241 (2009).
[3] T. Ritz, A. Damjanović, and K. Schulten, Chem. Phys. Chem. **3**, 243 (2002).
[4] G. R. Fleming and G. D. Scholes, Nature **431**, 256 (2004).
[5] P. Rebentrost, M. Mohseni, and A. Aspuru-Guzik, J. Phys. Chem. B **113**, 9942 (2009).
[6] A. Olaya-Castro and G. D. Scholes, Int. Rev. Phys. Chem. **30**, 49 (2011). 2967
[7] A. Ishizaki, T. R. Calhoun, G. S. Schlau-Cohen, and G. R. Fleming, Phys. Chem. Chem. Phys. **12**, 7319 (2010).
[8] G. R. Fleming, G. D. Scholes, and Y.-C. Cheng, Procedia Chemistry **3**, 38 (2011).
[9] G. S. Engel, T. R. Calhoun, E. L. Read, T.-K. Ahn, T. Mancal, Y.-C. Cheng, R. E. Blankenship, and G. R. Fleming, Nature 446, 782 (2007).
[10] G. D. Scholes, J. Phys. Chem. Lett. **1**, 2 (2010).
[11] G. Panitchayangkoon, D. Hayes, K. A. Fransted, J. R. Caram, E. Harel, J. Wen, R. E. Blankenship, and G. S. Engel, Proc. Natl. Acad. Sci. **107**, 12766 (2010).
[12] E. Collini, C. Y. Wong, K. E. Wilk, P. M. G. Curmin, P. Brumer, and G. D. Scholes, Nature Letters **463**, 644 (2010).
[13] T. R. Calhoun and G. R. Fleming, Phys. Status Solidi B **248**, 833 (2011).
[14] E. Harel and G. S. Engel, Proc. Natl. Acad. Sci. **109**, 706 (2012).
[15] G. R. Fleming, G. S. Schlau-Cohen, K. Amarnath, and J. Zaks, Faraday Discuss. **155**, 27 (2012).
[16] J. Strümpfer, M. Şener, and K. Schulten, J. Phys. Chem. Lett. **3**, 536 (2012).
[17] D. Egorova, M. F. Gelin, and W. Domcke, J. Chem. Phys. **126** 074314 (2007).
[18] D. B. Turner, K. E. Wilk, P. M. G. Curmi, and G. D. Scholes, J. Phys. Chem. Lett. **2**, 1904 (2011).
[19] J. Yuen-Zhou, J. J. Krich, and A. Aspuru-Guzik, J. Chem. Phys. **136**, 234501 (2012).
[20] V. Butkus, D. Zigmantas, L. Valkunas, and D. Abramavicius, Chem. Phys. Lett. **545**, 40 (2012).
[21] V. Butkus, L. Valkunas, and D. Abramavicius, J. Chem. Phys. **137**, 044513 (2012).
[22] J.-L. Brédas and R. Silbey, Science **323**, 48 (2009).
[23] E. Collini and G. D. Scholes, Science **323**, 369 (2009).
[24] I. Hwang and G. D. Scholes, Chem. Mater. **23**, 610 (2011).
[25] G. D. Scholes, Procedia Chemistry **3**, 82 (2011).
[26] G. D. Scholes, Chem. Phys. **275**, 373 (2002).
[27] G. D. Scholes, G. R. Flemming, A. Olaya-Castro, and R. van Grondelle, Nature Chem. **3** 763 (2011).
[28] S. Jang, Y.J. Jung, and R. J. Silbey, Chem. Phys. **275**, 319 (2002).
[29] M. Yang and G. R. Fleming, Chem. Phys. **275**, 355 (2002).
[30] S. Jang, Y.-C. Cheng, D. R. Reichnam, and J. D. Eaves, J. Chem. Phys. **129**, 101104 (2008).
[31] A. Ishizaki and G. R. Fleming, J. Chem. Phys. **130**, 234110 (2009).
[32] A. Ishizaki and G. R. Fleming, J. Chem. Phys. **130**, 234111 (2009).
[33] J. Olšina and T. Mančal, J. Mol. Model. **16**, 1765 (2010).
[34] A. Kolli, A. Nazir, and A. Olaya-Castro, J. Chem. Phys. **135**, 154112 (2011).
[35] R. Silbey, Procedia Chemistry **3**, 188 (2011).
[36] E. Runge and E. K. U. Gross, Phys. Rev. Lett. **52**, 997 (1984).
[37] E. K. U. Gross, J. F. Dobson, and M. Petersilka, in *Density Functional Theory*, edited by R. F. Nalewajski, Top. Curr. Chem. (Springer, Berlin, 1996), Vol. 181, p. 81.
[38] K. Yabana and G. F. Bertsch, Phys. Rev. B **54**, 4484 (1996).
[39] K. Yabana and G. F. Bertsch, Int. J. Quantum Chem. **75**, 55 (1999).
[40] M. A. L. Marques and E. K. U. Gross, Annu. Rev. Phys. Chem. **55**, 427 (2004).
[41] M. A. L. Marques, N. T. Maitra, F. M. S. Nogueria, E. K. U. Gross, and A. Rubio (Eds.), *Fundamentals of Time-Dependent Density Functional Theory (Lecture Notes in Physics)* (Springer Verlag, Berlin, 2012).
[42] T. Yanai, D. P. Tew, and N. C. Handy, Chem. Phys. Lett. **393**, 51 (2004).
[43] J.-D. Chai and M. Head-Gordon, J. Chem. Phys. **128**, 084106, (2008).
[44] E. Livshits and R. Baer, Phys. Chem. Chem. Phys. **9**, 2932 (2007).
[45] T. Stein, L. Kronik, and R. Baer, J. Am. Chem. Soc. **131**, 2818 (2009).
[46] A. Karolewski, T. Stein, R. Baer, and S. Kümmel, J. Chem. Phys. **134**, 151101 (2011).
[47] T. Körzdörfer, J. S. Sears, C. Sutton, and J.-L. Brédas, J. Chem. Phys. **135**, 204107 (2011).
[48] D. Hofmann, T. Körzdörfer, and S. Kümmel, Phys. Rev. Lett. **108**, 146401 (2012).
[49] K. Burke, R. Car, and R. Gebauer, Phys. Rev. Lett. **94**, 146803 (2005).
[50] M. Di Ventra and R. D'Agosta, Phys. Rev. Lett. **98**, 226403 (2007).
[51] R. D'Agosta and M. Di Ventra, Phys. Rev. B **78**,165105 (2008).
[52] H. Appel and M. Di Ventra, Phys. Rev. B **80** 212303 (2009).
[53] H. Appel and M. Di Ventra, Chem. Phys. **391**, 27 (2011).
[54] R. Biele and R. D'Agosta, arXiv:1112.2694v1 (2011).
[55] H. Appel, in *Fundamentals of Time-Dependent Density Functional Theory*, Chap. 11 (Springer Verlag, Berlin, 2012).
[56] N. Bushong and M. Di Ventra, J. Phys.: Condens. Matter **20**, 395214 (2008).
[57] Yu. V. Pershin, Y. Dubi, and M. Di Ventra, Phys. Rev. B **78**, 054302 (2008).
[58] J. Yuen-Zhou, C. Rodríguez-Rosario, and A. Aspuru-Guzik, Phys. Chem. Chem. Phys. **11**, 4509 (2009).
[59] R. D'Agosta and M. Di Ventra, arXiv:0911.3932v1 (2009).
[60] J. Yuen-Zhou, D. G. Tempel, C. A. Rodríguez-Rosario, and A. Aspuru-Guzik, Phys. Rev. Lett. **104**, 043001 (2010).
[61] D. G. Tempel and A. Aspuru-Guzik, Chem. Phys. **391**, 130 (2011).
[62] D. G. Tempel, M. A. Watson, R. Olivares-Amaya, and A. Aspuru-Guzik, J. Chem. Phys. **134** 074116 (2011).

[63] X. Zheng, C. Yam, F. Wang, and G. Chen, Phys. Chem. Chem. Phys. **13**, 14358 (2011).
[64] D. G. Tempel, J. Yuen-Zhou, and A. Aspuru-Guzik, in *Fundamentals of Time-Dependent Density Functional Theory*, Chap. 10 (Springer Verlag, Berlin, 2012).
[65] J. Dalibard, Y. Castin, and K. Mølmer, Phys. Rev. Lett. **68**, 580 (1992).
[66] P. Gaspard and M. Nagaoka, J. Chem. Phys. **111**, 5676 (1999).
[67] H.-P. Breuer and F. Petruccione, *The Theory of Open Quantum Systems* (Clarendon Press, Oxford, 2006).
[68] N. G. van Kampen, *Stochastic Processes in Physics and Chemistry*, third ed. (Elsevier, Amsterdam, 2007).
[69] U. Weiss, *Quantum Dissipative Systems*, third ed. (World Scientific, Singapore, 2008).
[70] G. W. Ford and R. F. O'Connell, Ann. Phys. **319**, 348 (2005).
[71] W. R. Frensley, Rev. Mod. Phys. **62**, 745 (1990).
[72] R. van Leeuwen, Phys. Rev. Lett. **82**, 3863 (1999).
[73] G. Vignale, Phys. Rev. B **70**, 201102(R) (2004).
[74] R. D'Agosta and G. Vignale, Phys. Rev. B **71**, 245103 (2005).
[75] D. Hofmann, PhD-Thesis, University of Bayreuth, submitted (2012).
[76] C. W. Gardiner, A. S. Parkins, and P. Zoller, Phys. Rev. A **46**, 4363 (1992).
[77] H.-P. Breuer and F. Petruccione, Phys. Rev. E **52**, 428 (1995).
[78] M. Mundt, S. Kümmel, Phys. Rev. B **76**, 035413 (2007).
[79] M. Mundt, J. Theor. Comput. Chem. **8**, 561 (2009).
[80] L. Kronik et al., Phys. status solidi B **243**, 1063 (2006).
[81] D. Hofmann, T. Körzdörfer, and S. Kümmel, Phys. Rev. A **82**, 012509 (2010).
[82] G. D. Scholes, Annu. Rev. Phys. Chem. **54**, 57 (2003).
[83] C. König and J. Neugebauer, Chem. Phys. Chem. **13**, 386 (2012).
[84] C.-Y. Wong and H. H. K. Tang, Phys. Rev. C **20**, 1419 (1979).
[85] All calculations are based on the local density approximation (LDA). We used real-space grids with a grid spacing of 0.7 bohr, a propagation time step of 0.001 fs, and norm conserving LDA pseudopotentials of Troullier-Martins [86] type (core cut-off radius r_c(Na)=3.09 bohr).
[86] N. Troullier and J. L. Martins, Phys. Rev. B **43**, 1993 (1991).
[87] J. Neugebauer, J. Phys. Chem. B **112**, 2207 (2008).
[88] C. Cohen-Tannoudji, B. Diu, and F. Laloë, *Quantenmechanik Band 1* (Walter de Gruyter, 2009), p. 374.